Supporting Information Section

Impacts of Trace Level Chromium on Formation of Superoxide within Uranyl Triperoxide Complexes

Sarah K. Scherrer, Harindu Rajapaksha, Dmytro V. Kravchuk, Sara E. Mason, and Tori Z. Forbes*

Table of Contents

Experimental Methods

Material Synthesis

All aqueous solutions were prepared using Millipore water (18.2 MΩ) and chemicals purchased were initially used without further purification. *Caution: $UO_2(NO_3)_2 \cdot 6H_2O$ contains radioactive ^{238}U, which is an α emitter, and like all radioactive materials must be handled with care. These experiments were conducted by trained personnel in a licensed research facility with special precautions taken toward the handling, monitoring, and disposal of radioactive materials.* **KUT-1** was synthesized and isolated as previously reported for **KUPS-1**.[1] In batches of 30 to 50 synthetic vials, 0.2 mL of 0.05 M uranyl dinitrate hexahydrate (International Bio-Analytical Industries Inc., 99.99%) in methanol was combined with 0.15 mL of pure methanol (Fischer Chemical, ACS 99.9%) and 2.5 mL of benzyl alcohol (Alfa Aesar, 99%) in a 20 mL scintillation vial. A separate aqueous solution containing 0.2 mL of 0.9 M aqueous potassium hydroxide (Sigma-Aldrich, 90%), 0.3 mL of 0.05 M aqueous *N*-(phosphonomethyl)iminodiacetic acid hydrate (Sigma-Aldrich, 95%) with potassium hydroxide for solubility, and 0.2 mL of 30% aqueous H_2O_2 (Fisher Chemical, ACS 99.9%) was mixed via vortex and carefully layered on top of the organic layer. The scintillation vials were capped and stored in the dark for overnight crystallization.

To isolate the **KUT-1** solid, the contents of each scintillation vial were transferred to a 15 mL plastic conical tube and centrifuged at 5000 rpm for 5 minutes. Each conical tube was decanted followed by the addition of 5 mL methylene chloride (Fisher Chemical, >99.5%). The conical tubes were centrifuged for an additional 5 minutes at 5000 rpm ensuring any residual water was forced into the top aqueous layer. The aqueous layer was decanted and the **KUT-1** solid was transferred to a watch glass for vacuum desiccator drying.

Purification of the uranyl dinitrate hexahydrate starting material

Following identification of contaminant chromium within the **KUT-1** complex, the uranyl dinitrate hexahydrate starting material was purified via a simple liquid-liquid extraction followed by back-extraction to recover the purified material. The liquid-liquid extraction was performed with an aqueous layer consisting of the uranyl dinitrate hexahydrate solid dissolved in 6 M HNO_3

and an organic layer consisting of 30% tributyl phosphate (TBP) in dodecane. After extraction of uranyl dinitrate to the organic layer, the aqueous layer was discarded. Recovery of the purified uranyl dinitrate was accomplished through a series of back-extractions using 2% HNO_3 and slow evaporation recrystallization. Once crystallized and dried fully, 0.05 M uranyl dinitrate hexahydrate in methanol was prepared and the **KUT-1** complex was synthesized as described above, now using the purified uranyl dinitrate hexahydrate stock solution.

Materials Characterization

Samples were characterized for purity using X-ray diffraction and Raman spectroscopy. Powder X-ray Diffraction data was collected on a Bruker D8 Advance diffractometer with nickel filtered Cu Kα radiation (λ =. 1.5418 Å), voltage 40 kV and current 40 mA in the continuous mode scanning from 5-60° 2θ with a step size of 0.05°. Samples were ground to a fine powder in a mortar and pestle and loaded on the sample holder equipped with a zero-background silica plate.

Raman spectra of solid and solution samples were collected on a SnRI High-Resolution Sierra 2.0 Raman Spectrometer equipped with a 785 nm laser and 2048 pixels TE-cooled detector. All spectra were acquired in three iterations with maximum laser energy of 15 mW for optimal resolution (2 cm^{-1}). Solid-state spectra were collected utilizing the orbital raster scan to focus on a larger area while maintaining high resolution, and an integration time of 5 seconds. Solution spectra did not require the raster scan feature and were collected with an integration time of 60 seconds to maximize signal intensity. The three iterations per sample were averaged and normalized by the appropriate laser power and integration time. Background subtraction was completed using PreDICT 64-bit software. Peak fitting and analysis were performed in Origin 9.60 (OriginLab, Northampton, MA) 64-bit software using Lorentzian or Gaussian function peak analysis protocols.

Inductively coupled plasma mass spectrometry (ICP-MS) was utilized to evaluate the presence of contaminant chromium species in the starting materials, namely uranyl nitrate hexahydrate and potassium hydroxide. Data was collected on a 7800 Agilent inductively coupled plasma mass spectrometer. The instrument used a helium carrier gas in low matrix mode and no collision gas was used. Five calibration standard solutions (0, 10, 100, 1000 and 2000 ppb Cr in 2% HNO_3) were prepared through a series of dilutions from the NIST chromium ICP standard (Sigma-Aldrich, 1000 mg/L $Cr(NO_3)_3$ in 2-3% HNO_3). 10mL samples of the uranyl nitrate

hexahydrate and potassium hydroxide solids were each acidified in 2% HNO_3 for triplicate analysis. Additional data was collected with the purified uranyl nitrate material.

Continuous Wave X-band EPR spectroscopy

Continuous-wave X-band EPR spectroscopy was utilized for both solid-state and solution samples. Spectra were collected at room temperature using a Bruker EMX EPR spectrometer. Solid samples were loaded in a 200 mm x 4 mm quartz EPR tube. Solution samples were prepared by dissolving 100 mg **KUT-1** in 4.5 mL distilled H_2O yielding a 30 mM **KUPS-1** solution. Additional control experiments were completed using 0.9 M potassium hydroxide (KOH) and 30% hydrogen peroxide (H_2O_2). For spin trapping studies, a separate mixture of 0.12 mL H_2O and 0.05 mL 5,5-Dimethyl-1-Pyrroline-N-Oxide (DMPO) were mixed via vortex. Addition of 0.83 mL 30 mM **KUPS-1** yielded a solution that contained 25 mM **KUPS-1** and 50 mM DMPO. A capillary tube was filled with each sample solution, sealed from air using capillary tube sealing wax, and placed inside a quartz EPR tube capped with a septa. Operating parameters (microwave power, modulation amplitude) were optimized for each sample at time zero. The same operating parameters were utilized for the respective sample at each time frame collected. Modulation frequency was set to 100 kHz for all collections and frequency was 9.85 GHz. Magnetic field values were converted to *g*-factors and subsequent spectral analysis was performed using standard protocol. Data was plot in Origin 9.60 (OriginLab, Northampton, MA) 64-bit software and simulated in MATLAB using EasySpin.[2]

Density Functional Theory Calculations

All the DFT calculations of radical species were open-shell and unrestricted. The Gaussian 16 software package[3] was used to perform all geometry optimizations and frequency calculations. To model exchange correlation effects, the B3-LYP (Becke, 3-parameter, Lee-Yang-Parr)[4, 5] hybrid function was used. The Van Der Waals dispersion correction methods DFT-D3 with the Becke-Johnson damping term were utilized.[6,7,8] The polarized triple zeta (def2-TZVP)[9] basis set was utilized to represent the O, and H atoms, while the ECP60MWB and ECP60MWB-SEG pseudopotential was used for U.[10,11] Scalar relativistic effects are included by employing small-core Effective Core Potentials (ECPs), while spin–orbit effects are ignored. The Ultrafine integration grid was used in all the calculations. All structures were optimized with no symmetry

constrained to a tight convergence criterion (Root Mean Square (RMS) force criterion of 1×10^{-5} Hartrees per radians). The calculated vibrational frequencies were monitored to ensure that structures get optimized to a true minimum with no negative frequencies.

g-tensor calculations of the optimized structures were performed by ORCA 5.0.4.[12] using B3-LYP[4, 5] hybrid functional. Relativistic effects are included by Zeroth-Order Regular Relativistic Approximation (ZORA)[13,14] in combination with ZORA-recontracted[15] versions of the def2 basis sets.[16,17] H and O atoms are represented by ZORA-def2-TZVP basic set while U atoms are represented by SARC-ZORA-TZVP basic set together with SARC/J coulomb-fitting auxiliary base sets.[14-17] Defgrid3 integration grid was used in all the calculation. Visualization of spin densities was done using Chemcraft program.[18]
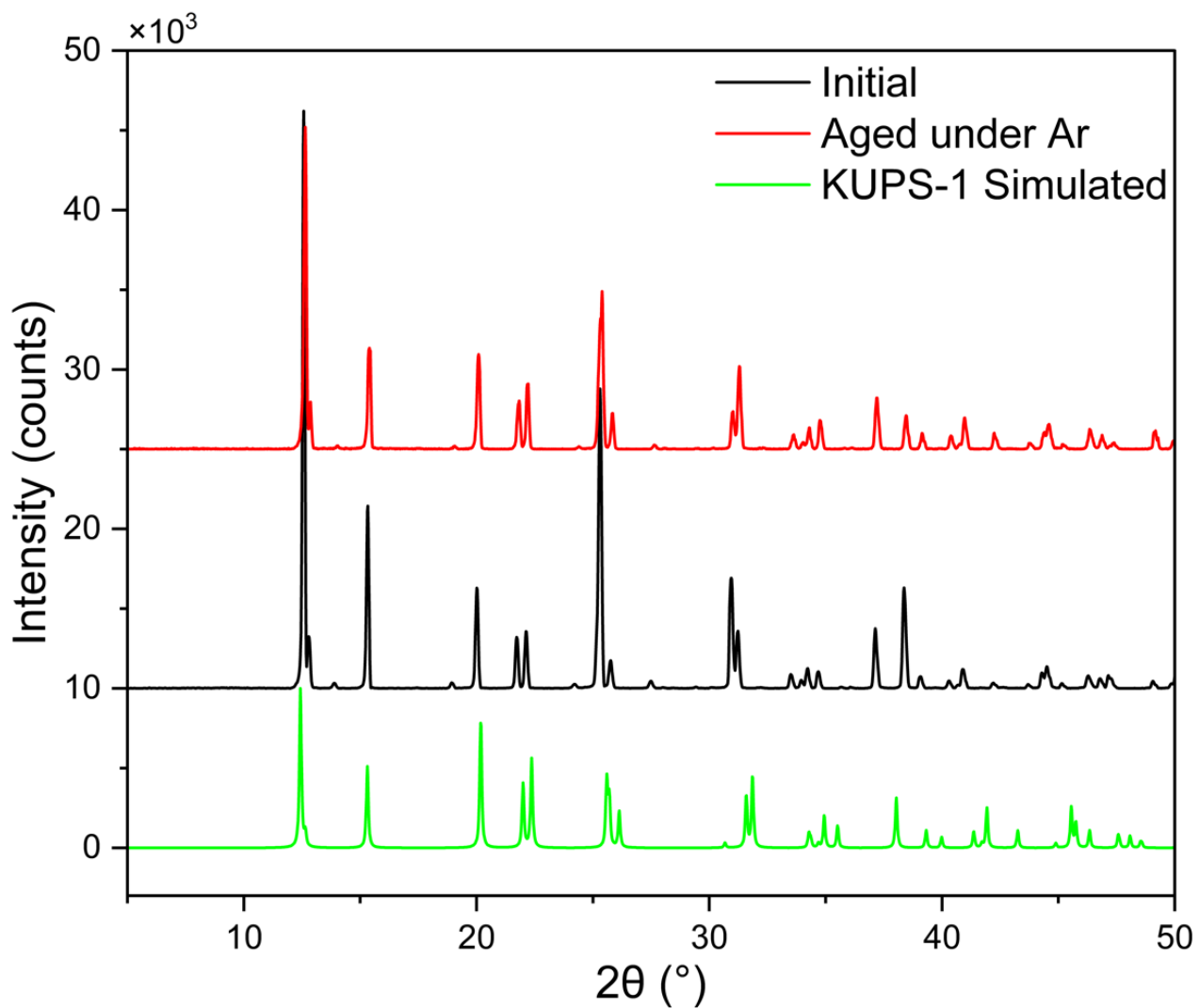
Materials Characterization

Figure S1. Representative Powder X-ray diffraction of **KUT-1** (black trace) and **KUPS-1** (red trace) compound. The simulated pattern was obtained from the reported crystal structure (ICSD 135984).[1]
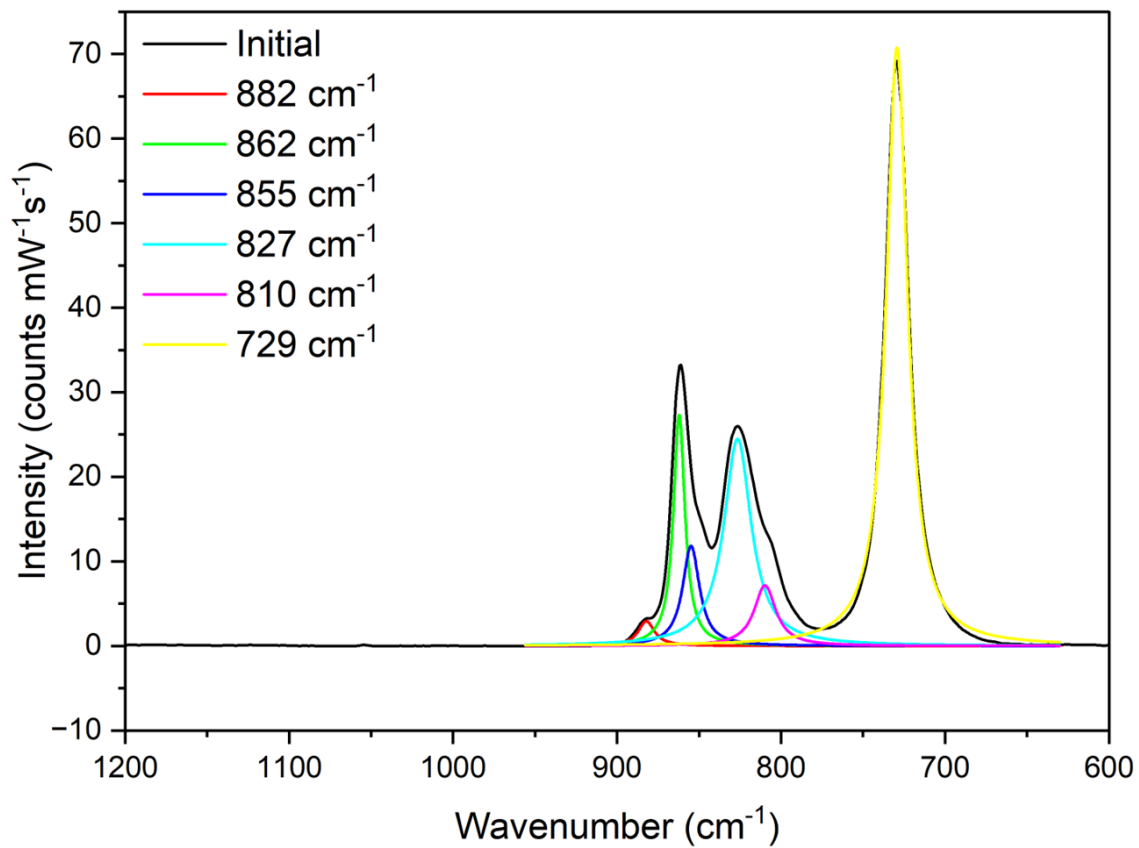
Figure S2. Fitted Raman spectrum of **KUT-1** compound.

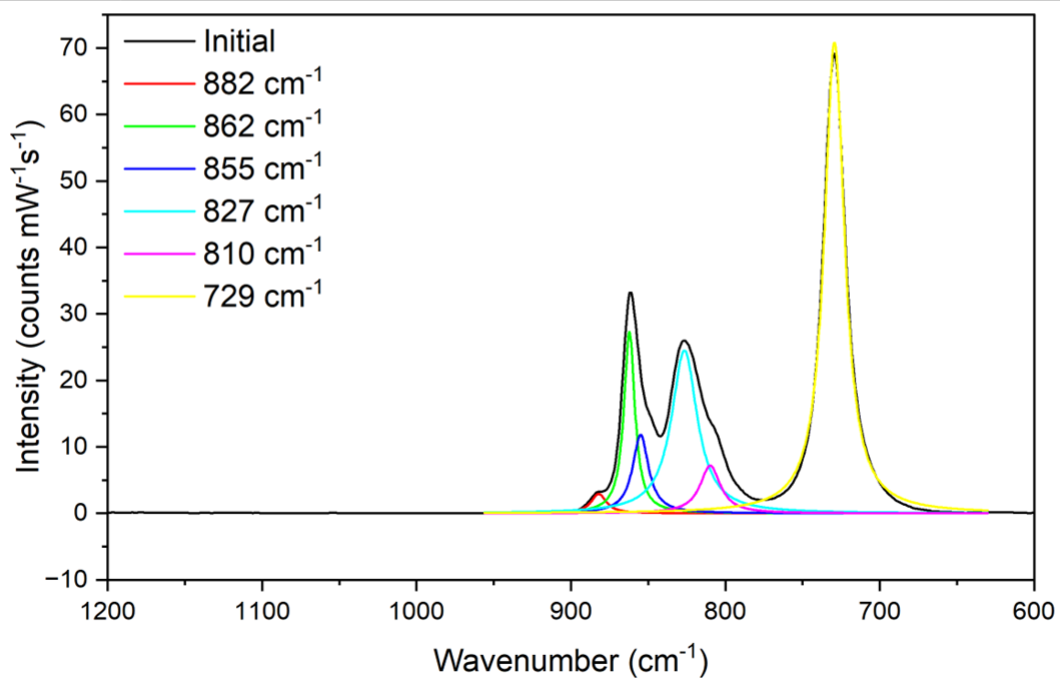| Model	Lorentz					
Equation	y = y0 + (2*A/pi)*(w/(4*(x-xc)^2 + w^2))					
Plot	Peak1(Intensity)	Peak2(Intensity)	Peak3(Intensity)	Peak4(Intensity)	Peak5(Intensity)	Peak6(Intensity)
y0	0 ± 0	0 ± 0	0 ± 0	0 ± 0	0 ± 0	0 ± 0
xc	882.0797 ± 1.101	862.16617 ± 0.2230	854.91779 ± 0.9537	826.5431 ± 0.317	809.81225 ± 0.857	729.40973 ± 0.05024
w	12 ± 0	8.48871 ± 0.68616	12.4765 ± 2.18394	20.25613 ± 1.21663	16.02027 ± 2.638	15.76682 ± 0.14361
A	55 ± 0	364.45655 ± 55.712	231.75999 ± 70.202	779.05454 ± 57.397	180.3158 ± 42.432	1752.91061 ± 11.351
Reduced Chi-S	1.25898					
R-Square (CO	0.99379					
Adj. R-Square	0.99349					

Figure S3. Fitting parameters for the Raman spectrum of **KUT-1** compound.
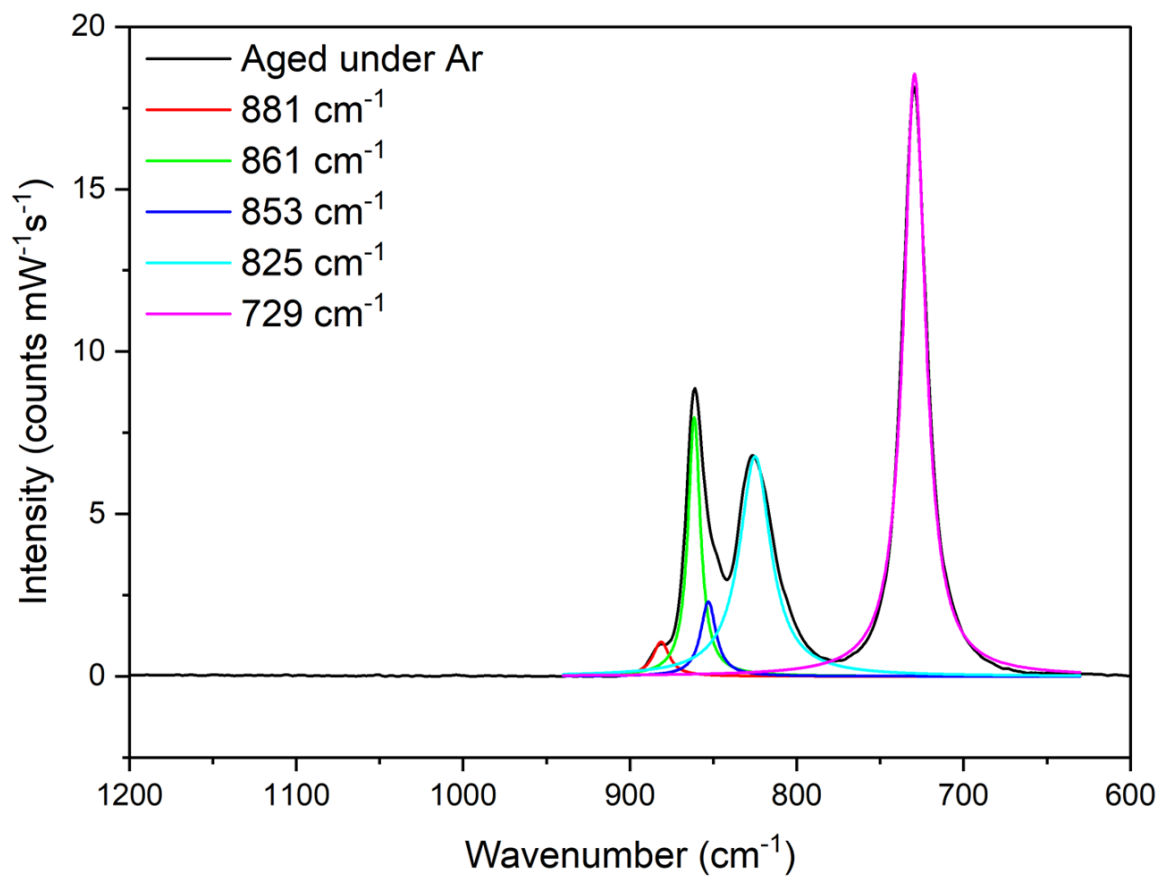
Figure S4. Fitted Raman spectrum of **KUPS-1** aged under argon for 3 weeks.

| Model	Lorentz				
Equation	y = y0 + (2*A/pi)*(w/(4*(x-xc)^2 + w^2))				
Plot	Peak1(Intensity)	Peak2(Intensity)	Peak3(Intensity)	Peak4(Intensity)	Peak5(Intensity)
y0	0 ± 0	0 ± 0	0 ± 0	0 ± 0	0 ± 0
xc	881.29796 ± 0.88452	861.44911 ± 0.12001	853 ± 0	824.98089 ± 0.20703	729.43257 ± 0.0566
w	12 ± 0	8.96829 ± 0.39589	11.13545 ± 1.75803	22.62772 ± 0.65721	16.1038 ± 0.16159
A	20 ± 0	112.37173 ± 5.21826	40.19201 ± 7.09482	240.57033 ± 5.67314	469.44599 ± 3.34638
Reduced Chi-Sqr	0.10758				
R-Square (COD)	0.99249				
Adj. R-Square	0.99221				
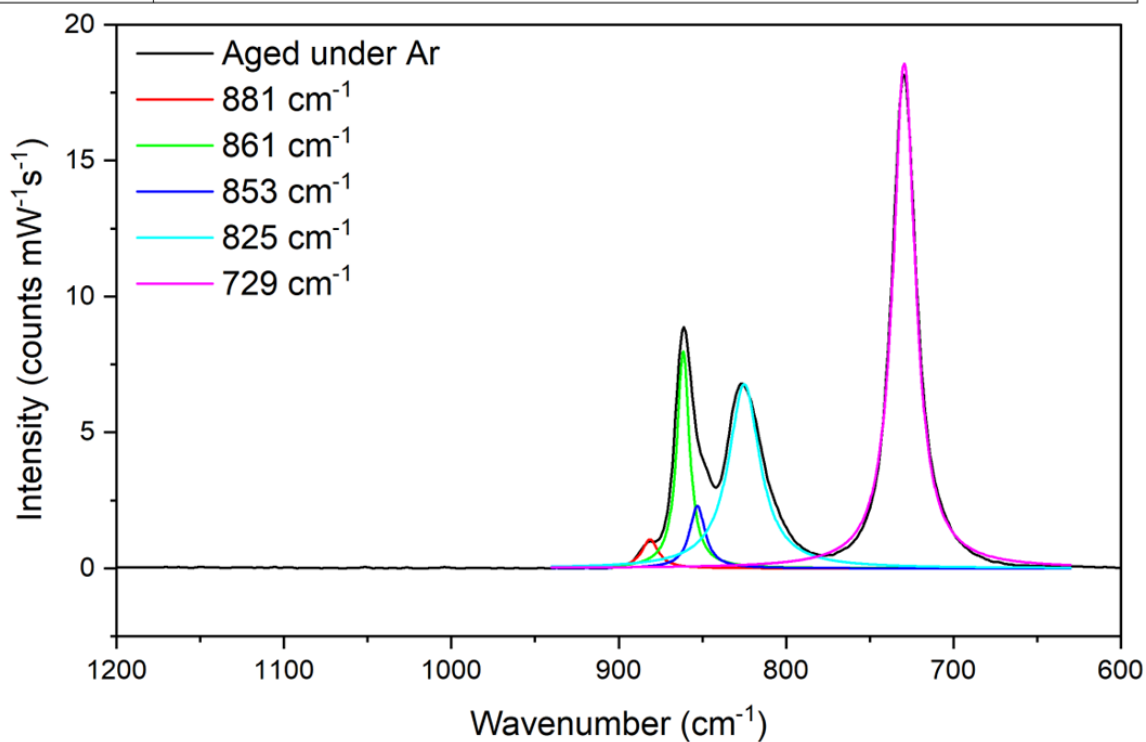
Figure S5. Fitting parameters for the Raman spectrum of **KUPS-1** aged under argon for 3 weeks.
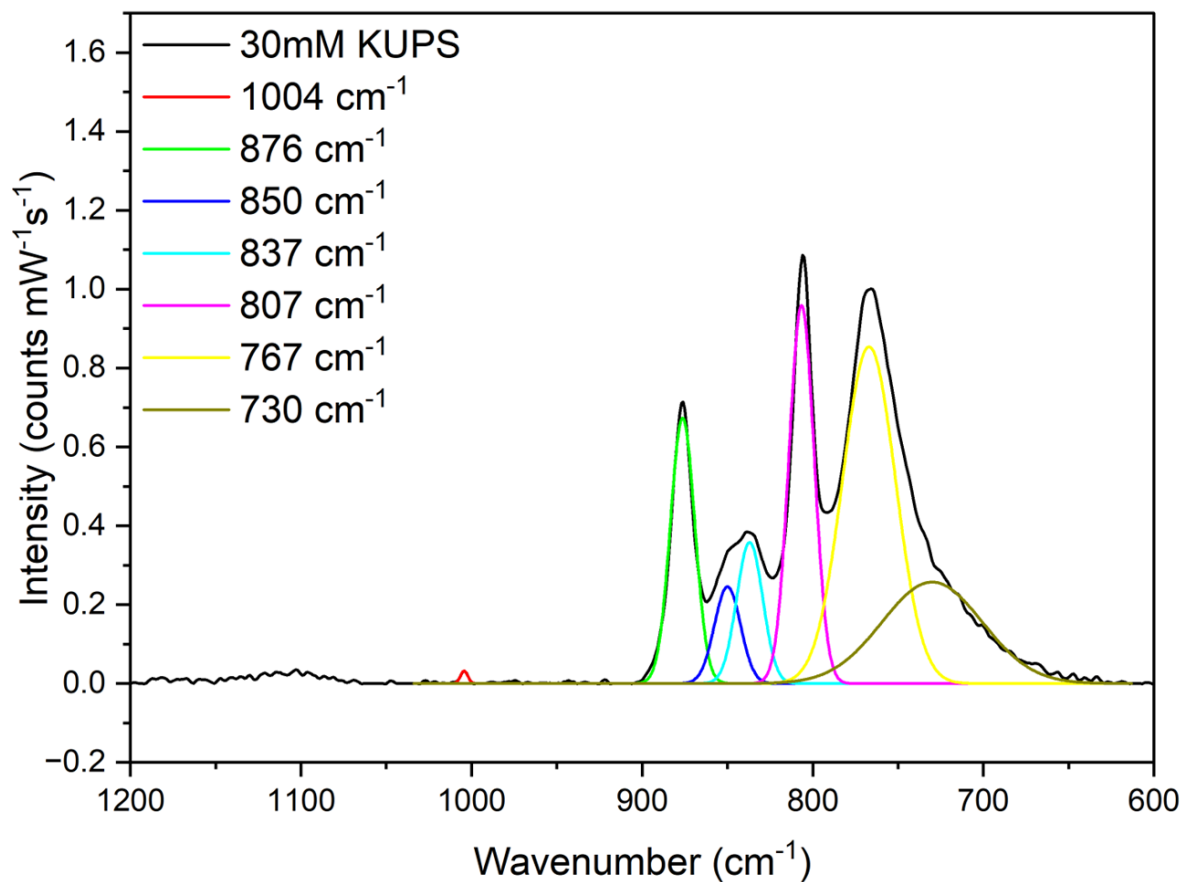
Figure S6. Fitted Raman spectrum of 30mM **KUPS-1**.

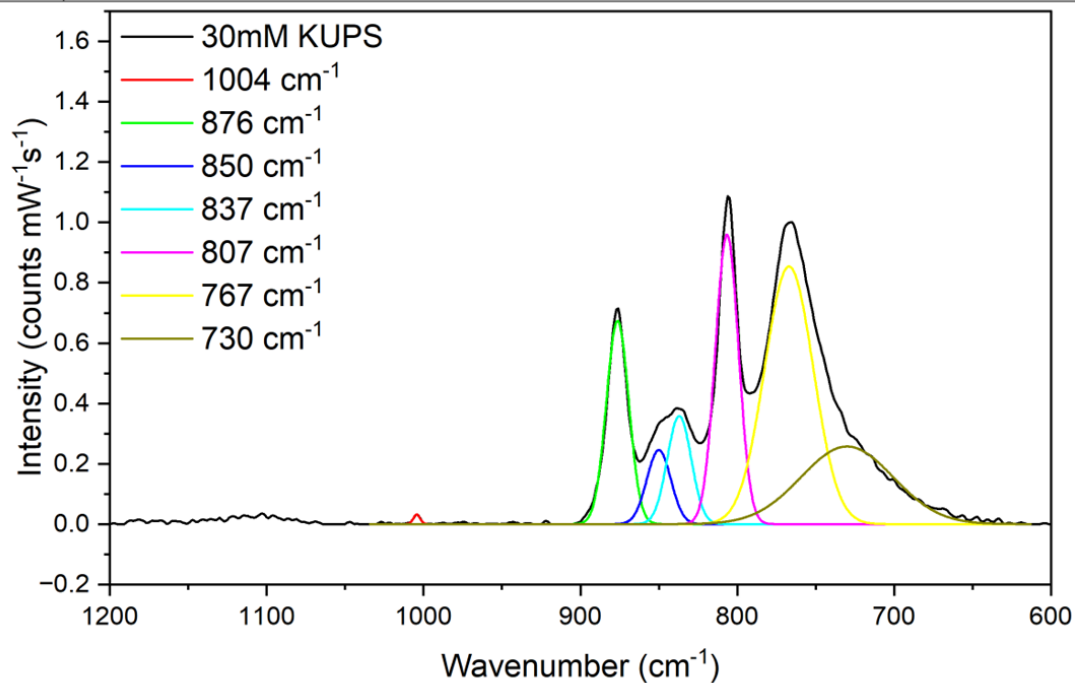| Model	Gaussian						
Equation	y = y0 + A/(w*sqrt(pi/(4*ln(2)))) * exp(-4*ln(2)*(x-xc)^2/w^2)						
Plot	Peak1(Intensity)	Peak2(Intensity)	Peak3(Intensity)	Peak4(Intensity)	Peak5(Intensity)	Peak6(Intensity)	Peak7(Intensity)
y0	0 ± 0	0 ± 0	0 ± 0	0 ± 0	0 ± 0	0 ± 0	0 ± 0
xc	1004.35224 ± 1.40	876.30479 ± 0.122	850 ± 0	837 ± 0	806.57818 ± 0.098	767.02191 ± 0.182	730 ± 0
A	0.16869 ± 0.09686	12.0183 ± 0.17964	4.70206 ± 0.176	6.86126 ± 0.174	17.74343 ± 0.2367	33.18503 ± 0.4103	18.91981 ± 0.517
w	4.99732 ± 3.31347	16.76984 ± 0.2917	18 ± 0	18 ± 0	17.38017 ± 0.2358	36.50201 ± 0.4868	69.09218 ± 2.112
Reduced Chi-S	8.31484E-4						
R-Square (CO	0.99023						
Adj. R-Square	0.98987						

Figure S7. Fitting parameters for the Raman spectrum of 30mM **KUPS-1**.
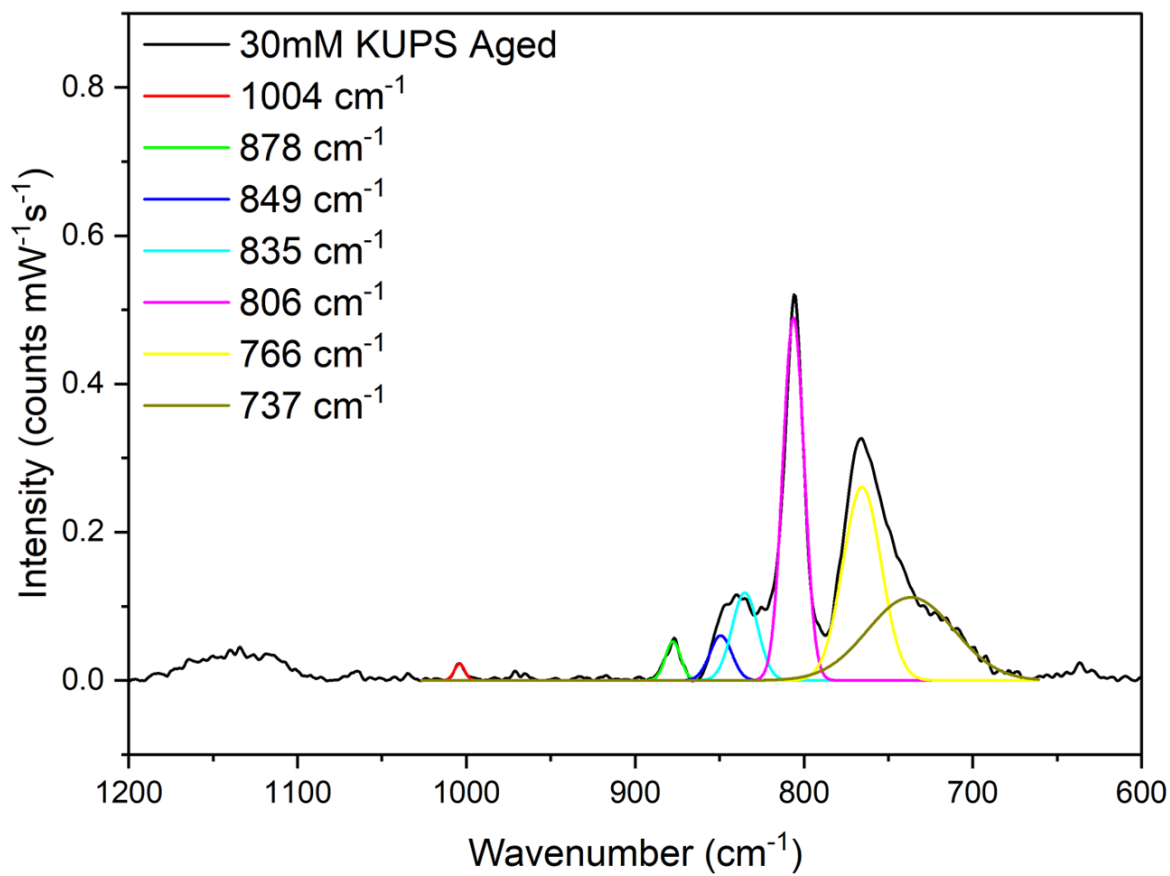
Figure S8. Fitted Raman spectrum of 30mM **KUPS-1** aged.

| Model	Gaussian						
Equation	y = y0 + A/(w*sqrt(pi/(4*ln(2)))) * exp(-4*ln(2)*(x-xc)^2/w^2)						
Plot	Peak1(Intensity)	Peak2(Intensity)	Peak3(Intensity)	Peak4(Intensity)	Peak5(Intensity)	Peak6(Intensity)	Peak7(Intensity)
y0	0 ± 0	0 ± 0	0 ± 0	0 ± 0	0 ± 0	0 ± 0	0 ± 0
xc	1004.03899 ± 0.88865	877.61187 ± 0.46492	849.27707 ± 0.48308	835 ± 0	806.22841 ± 0.05931	765.62193 ± 0.18096	736.60731 ± 0
A	0.1701 ± 0.04316	0.59463 ± 0.0528	0.99035 ± 0	2.26454 ± 0	7.67353 ± 0.06525	7.4496 ± 0.11755	7.19159 ± 0.17853
w	7.14159 ± 2.0926	10.67931 ± 1.09533	15.38615 ± 0	18 ± 0	14.73187 ± 0.14165	26.81511 ± 0.39875	60.32146 ± 1.62076
Reduced Chi-Sqr	1.15532E-4						
R-Square (COD)	0.98982						
Adj. R-Square	0.98942						
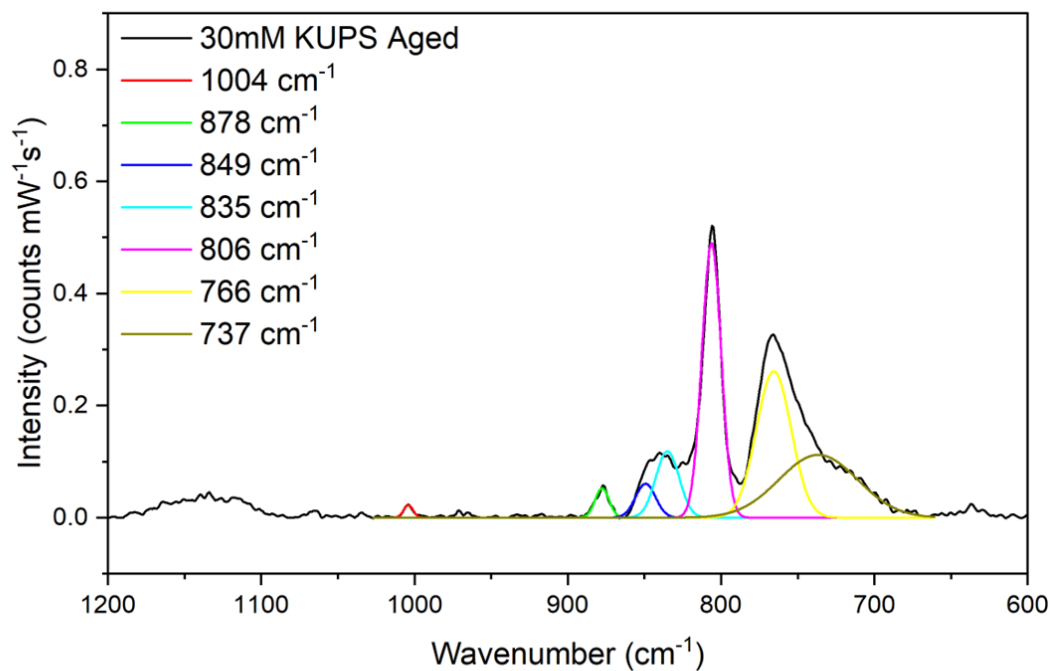
Figure S9. Fitting parameters for the Raman spectrum of 30mM **KUPS-1** aged.

Details of DFT Studies

Coordinates of DFT Optimized structures

Table S1: DFT optimized coordinate of $[UO_2(O_2)_2O_2{}^*]^{3-,2}$ shown in Å.

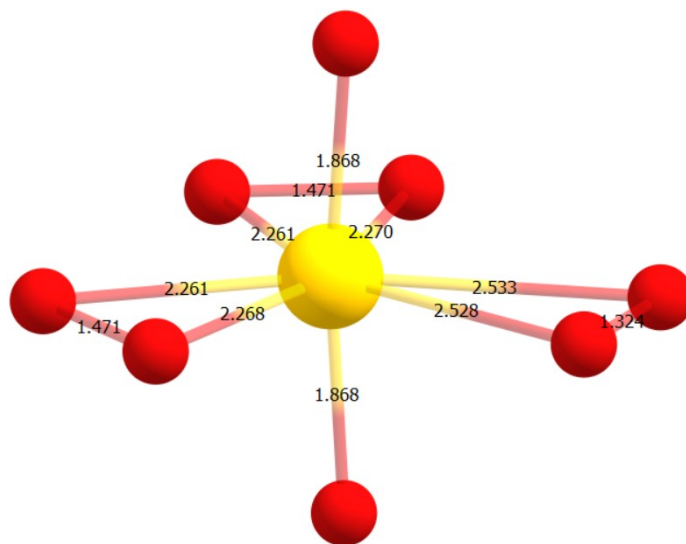|			
O	8.96490	2.30910	2.51910
O	5.70560	3.97670	1.84600
O	8.24350	4.11730	0.19820
O	8.45540	5.00020	1.35970
O	6.77990	3.07820	4.70910
O	7.41100	4.23810	4.52600
O	6.77500	1.41910	0.62490
O	6.31560	1.06890	1.98130
U	7.34970	3.11160	2.03480

Figure S10: DFT optimized bond lengths of $[UO_2(O_2)_2O_2{}^*]^{3-,2}$ shown in Å. For more information on the experimental crystal data, refer to CCDC ICSD 135984.[1]

Table S2: Calculated g-tensors for free oxygen-based radicals.

Radical	g_x	g_y	g_z	g_{iso}
$O_2^{\bullet-}$	2.0019	2.0090	2.1748	2.0619
$OH^{\bullet}$	2.0021	2.0079	2.0667	2.0256
$OOH^{\bullet}$	2.0020	2.0078	2.0308	2.0135

Solid-state EPR spectroscopy

Table S3. Known g-factors for superoxide phases.

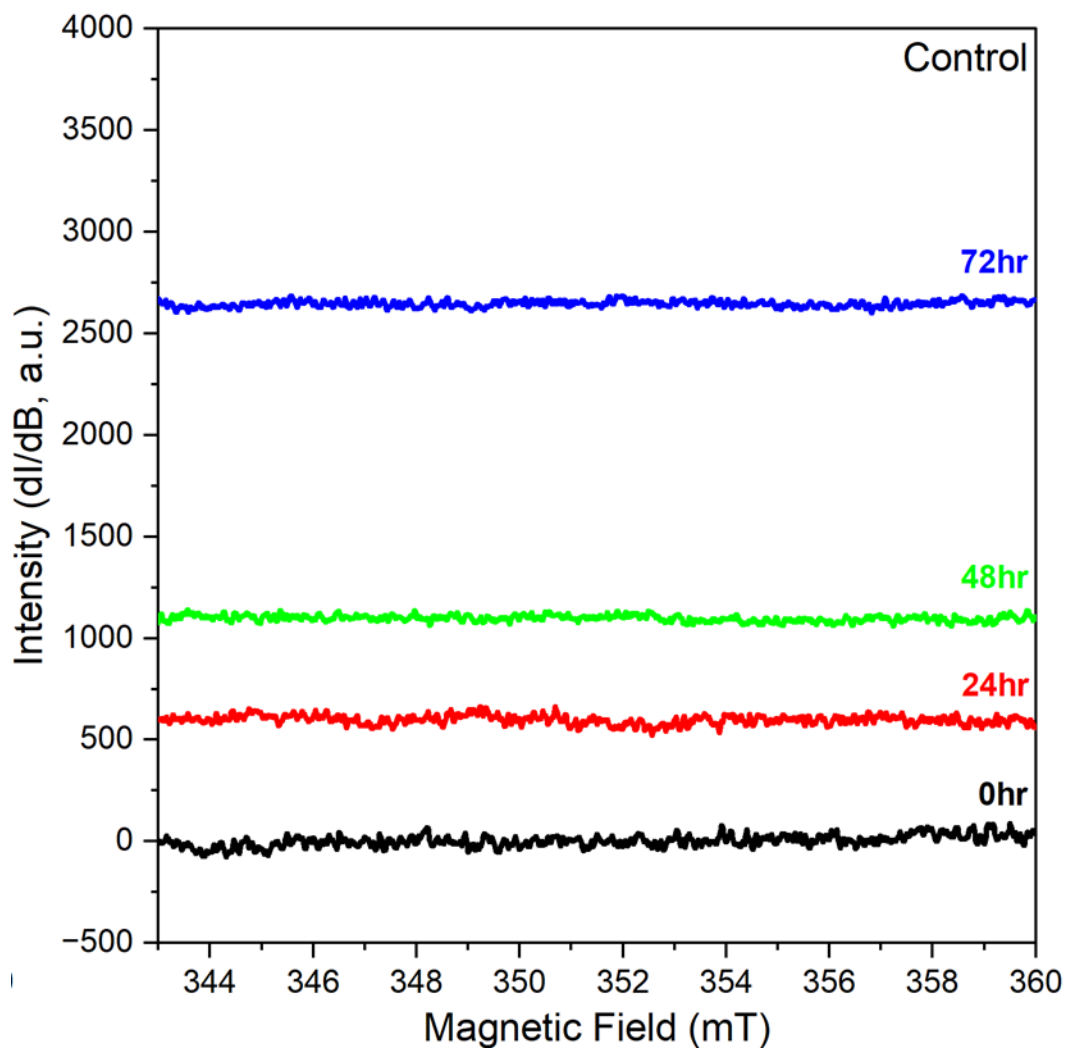| Phase	g_x	g_y	g_z	g_{iso}	Reference
NaO_2 (T = 10K)	2.0075	2.022	2.1106		[19]
KO_2 (T = 10K)	2.0068	2.0007	2.1184		[19]
CsO_2 (T = 10K)	2.0069	2.0013	2.1069		[19]
$[N(CH_3)_3(C_6H_5)](O_2)$ (T = 110K)	2.015	2.014	2.236	2.088	[20]
$[N(C_4H_9)_4](O_2)$ (T = 110K)	2.018	2.149	2.131	2.099	[20]

Solution-state EPR spectroscopy

Figure S11. EPR Spectroscopy of the control solution (0.1 mM H_2O_2, 0. 1mM KOH) over 72 hours without DMPO spin trap.
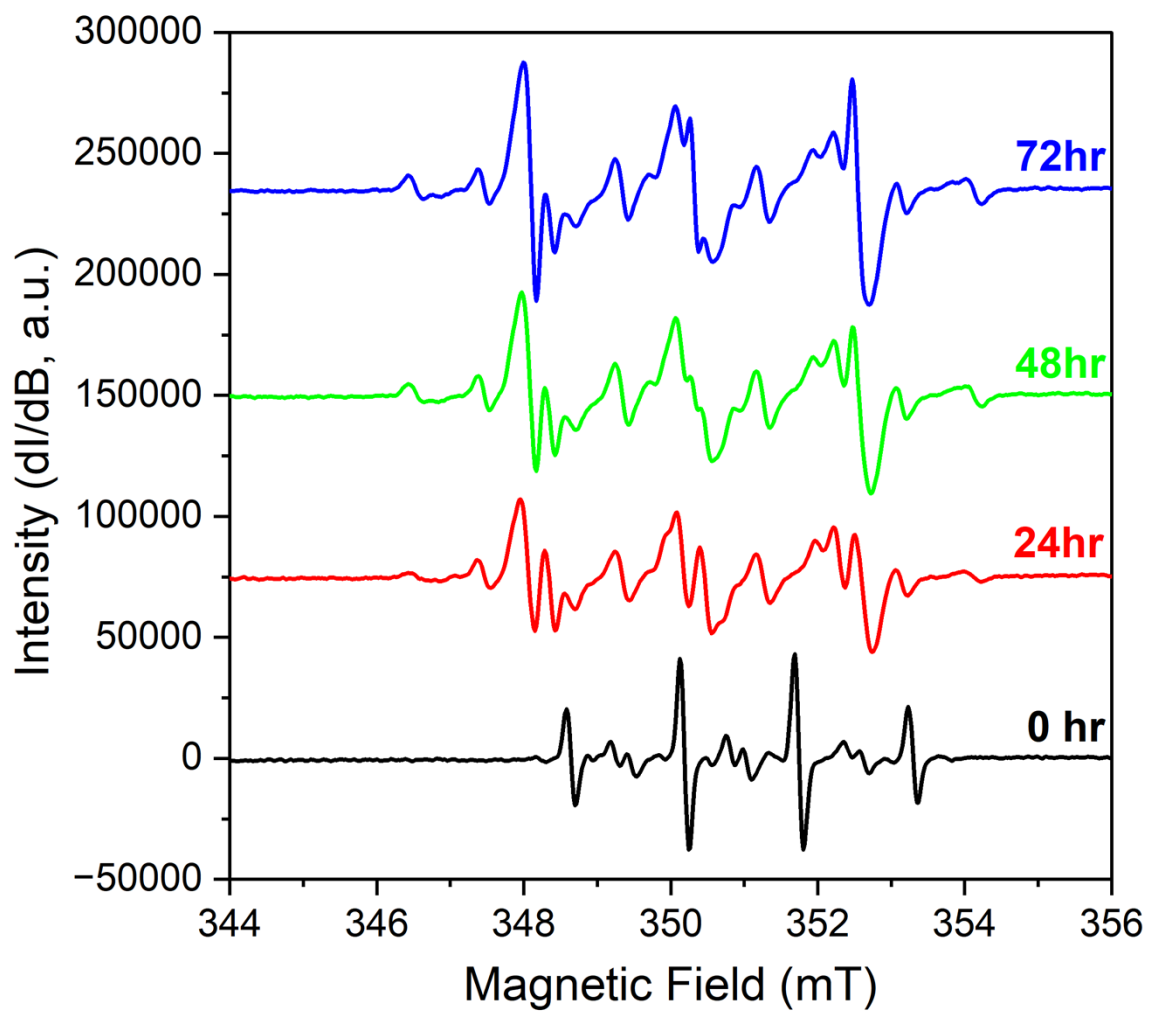
Figure S12. EPR Spectroscopy of the control solution (0.1 mM H_2O_2, 0. 1mM KOH, and 50 mM DMPO) over 72 hours.
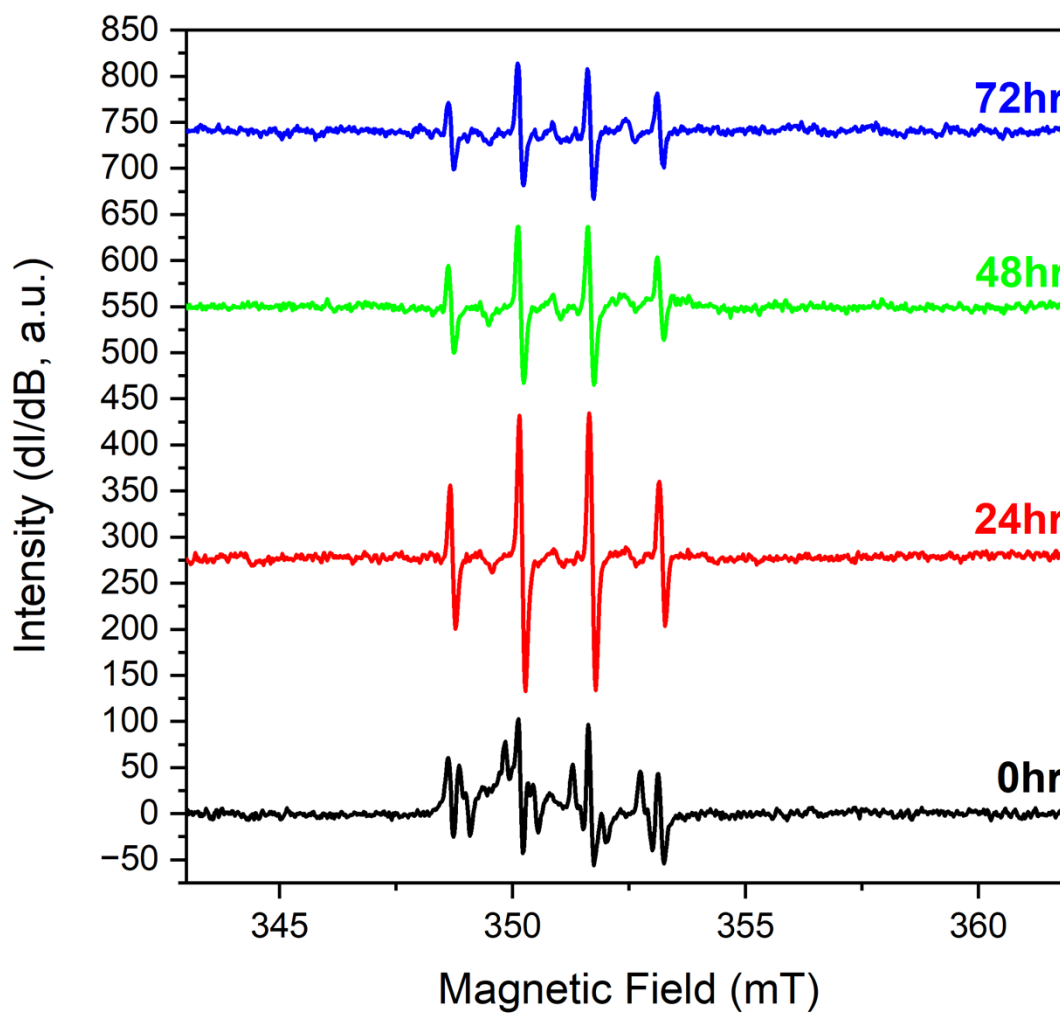
Figure S13. EPR spectra of 25mM **KUPS-1** (Cr purified) and 50mM DMPO over 72 hours.

Inductively Coupled Plasma Mass Spectrometry

Table S4. Inductively Coupled Plasma Mass Spectrometry analysis of Cr within the starting materials.

Sample	Cr Concentration (ppb)	Cr Concentration Relative Standard Deviation (%)
Uranyl dinitrate hexahydrate	263.4	10.4

Potassium hydroxide	58.9	10.8
Purified uranyl dinitrate hexahydrate	<0.000	N/A

References

(1) Kravchuk, D.V.; Dahlen, N.N; Kruse, S.J.; Malliakas, C.D.; Shand, P.M.; Forbes, T.Z. Isolation and Reactivity of Uranyl Superoxide. *Angew Chem Int Ed*, **2021**. *60*(27): p. 15041-15048.

(2) Stoll, S.; Schweiger, A. EasySpin, a comprehensive software package for spectral simulation and analysis in EPR. *Journal of Magnetic Resonance*, **2006**. *178*(1): p. 42-55.

(3) Frisch, M. J.; Trucks, G. W.; Schlegel, H. B.; Scuseria, G. E.; Robb, M. A.; Cheeseman, J. R.; Scalmani, G.; Barone, V.; Petersson, G. A.; Nakatsuji, H.; et al. Gaussian 16. **2009**.

(4) Becke, A. D. Density-functional thermochemistry. III. The role of exact exchange. *The Journal of Chemical Physics* **1993**, *98* (7), 5648-5652. DOI: 10.1063/1.464913.

(5) Lee, C.; Yang, W.; Parr, R. G. Development of the Colle-Salvetti correlation-energy formula into a functional of the electron density. *Physical Review B* **1988**, *37* (2), 785-789. DOI: 10.1103/PhysRevB.37.785.

(6) Becke, A. D.; Johnson, E. R. A density-functional model of the dispersion interaction. *The Journal of Chemical Physics* **2005**, *123*(15), 154101. https://doi.org/10.1063/1.2065267.

(7) Grimme, S.; Ehrlich, S.; Goerigk, L. Effect of the damping function in dispersion corrected density functional theory. *Journal of Computational Chemistry* **2011**, *32* (7), 1456-1465. DOI: https://doi.org/10.1002/jcc.21759.

(8) Grimme, S.; Antony, J.; Ehrlich, S.; Krieg, H. A consistent and accurate *ab initio* parametrization of density functional dispersion correction (DFT-D) for the 94 elements H-Pu. *The Journal of Chemical Physics* **2010**, *132* (15), 154104. DOI: https://doi.org/10.1063/1.3382344.

(9) Weigend, F.; Häser, M.; Patzelt, H.; Ahlrichs, R. RI-MP2: optimized auxiliary basis sets and demonstration of efficiency. *Chemical Physics Letters* **1998**, *294* (1), 143-152. DOI: https://doi.org/10.1016/S0009-2614(98)00862-8.

(10) Cao, X.; Dolg, M. Segmented contraction scheme for small-core actinide pseudopotential basis sets. *Journal of Molecular Structure: THEOCHEM* **2004**, *673* (1), 203-209. DOI: https://doi.org/10.1016/j.theochem.2003.12.015.

(11) Cao, X.; Dolg, M.; Stoll, H. Valence basis sets for relativistic energy-consistent small-core actinide pseudopotentials. *The Journal of Chemical Physics* **2003**, *118* (2), 487-496. DOI: 10.1063/1.1521431.

(12) Neese, F.; Wennmohs, F.; Becker, U.; Riplinger, C. The ORCA quantum chemistry program package. *The Journal of Chemical Physics* **2020**, *152* (22). DOI: 10.1063/5.0004608 (acccessed 10/7/2023).

(13) van Lenthe, E.; Baerends, E.-J.; Snijders, J. G. Relativistic regular two-component Hamiltonians. *The Journal of chemical physics* **1993**, *99* (6), 4597-4610.

(14) van Wüllen, C. Molecular density functional calculations in the regular relativistic approximation: Method, application to coinage metal diatomics, hydrides, fluorides and chlorides, and comparison with first-order relativistic calculations. *The Journal of chemical physics* **1998**, *109* (2), 392-399.

(15) Pantazis, D. A.; Chen, X.-Y.; Landis, C. R.; Neese, F. All-electron scalar relativistic basis sets for third-row transition metal atoms. *Journal of chemical theory and computation* **2008**, *4* (6), 908-919.

(16) Weigend, F.; Ahlrichs, R. Balanced basis sets of split valence, triple zeta valence and quadruple zeta valence quality for H to Rn: Design and assessment of accuracy. *Physical Chemistry Chemical Physics* **2005**, *7* (18), 3297-3305.

(17) Pantazis, D.A.; Neese, F. All-Electron Scalar Relativistic Basis Sets for the Actinides. *Journal of Chemical Theory and Computation* **2011**, *7* (3), 677-684. DOI: 10.1021/ct100736b.

(18) *Chemcraft*; 2009. https://www.chemcraftprog.com

(19) Lindsay, D.M.; Herschbach, D.R.; Kwiram, A.L. Matrix Isolated Alkali Superoxides. *Chemical Physics Letters* **1974**, *25*, 175-181.

(20) Dietzel, P.D. C.; Kremer, R.K.; Jansen, M. Tetraorganylammonium Superoxide Compounds: Close to Unperturbed Superoxide Ions in the Solid State. *Journal of the American Chemical Society* **2004**, *126* (14), 4689-4696. DOI: 10.1021/ja039880i.